Relationship between birefringence and surface morphology in single crystal diamonds grown by MPCVD

Yun Zhao, Yanzhao Guo, Liangzhen Lin, Yuting Zheng, Lifu Hei, Jinlong Liu, Junjun Wei, Liangxian Chen, Chengming Li*

(Institute for Advanced Materials and Technology, University of Science and Technology Beijing, Beijing 100083, China)

Abstract: Single-crystal diamonds were successfully synthesized using microwave plasma chemical vapor deposition (MPCVD). A smooth and flat single-crystal surface was obtained by optimizing the size relationship between the seed substrate and the square hole of the shielding ring. When the sample grows higher than the polycrystalline diamond on the molybdenum holder, the surface becomes uneven. The polarization characteristics of two kinds of CVD layers were compared between flat and uneven surfaces. Abnormally high-order birefringence occurs in both morphologies, which is related to the dislocations density in the CVD layers. The higher dislocation density of the sample, the more obvious high-order anomalous birefringence. High pressure high temperature (HPHT) seed substrates have obvious defects, such as dislocations, stacking faults and boundaries of the growth sector, and these defects are mostly distributed at the edge of seed substrates. When the diamond surface demonstrates an edge-to-center morphology, the dislocations in the seed substrate, interface-induced dislocations, and dislocations formed in the growth layer begin to converge toward the central region of the CVD layer, which results in a smaller area of low stress in the center of the CVD layer. High dislocation density causes the crystal to have a mosaic structure and orientation deviation.

Keywords: MPCVD, Diamond growth, Birefringence, Dislocations, X-ray topography.

1. Introduction

Microwave plasma chemical vapor deposition (MPCVD) is an established process that is currently the most important method for synthesizing single crystal diamonds [1,2]. In recent years, high-quality CVD single crystal diamonds have been used in high-end electronic devices, such as power diodes [3] and transistors [4], refractive lenses for synchrotron X-ray sources [5], Raman lasers [6], energetic particle detectors [7,8], magnetic sensors [9], and quantum information processors [10,11]. Currently, silicon is the preferred material for Bragg diffraction due to its effective size and because it provides the perfect lattice. However, diamond has a lower absorption coefficient than silicon, higher thermal conductivity, and a lower thermal expansion coefficient. If the perfection and size of diamonds could be improved, single crystal diamonds would replace silicon in the future [12,13]. Suppressing the defects in diamonds is key for using diamonds in next-generation semiconductor devices, thus motivating research on the basic theory of CVD single crystal growth diamonds. Currently, research on the basic theory of CVD diamond growth is mainly focused on the growth mechanism of CVD single crystal diamonds [14], nitrogen doping and its influence on the growth rate of single crystal diamonds [15-17], and

controlling defects in single crystal diamonds [18-20].

When single crystal diamonds are grown under high pressure and high power density, non-epitaxial features are sometimes formed on the top of the grown crystal, resulting in the formation of polycrystalline diamonds on the single crystal surface. In severe cases, cracks may occur due to stress [21]. The growth is stopped at this point, which will limit the size of the single crystal diamond. The geometry of the seed substrate and the discharge location of the plasma will affect the synthetic environment of the diamond and the final result of the single crystal synthesis [22]. If the microwave discharge is closer to the substrate, the discharge state of the plasma may change due to the presence of the substrate and the shape and size of the molybdenum holder. Thus, the diamond synthesis process can be changed by changing the size and shape of the molybdenum holder [23-25], and this change is realized by controlling the temperature distribution of the substrate [26]. It is necessary to optimize the geometric design of the molybdenum holder to change the local processing environment around the substrate and stabilize the growth environment to promote the growth of high-quality single crystal diamonds at high growth rates.

In this paper, a high-quality single crystal diamond was grown at a high growth rate by optimizing the geometric design of the molybdenum holder. The stress distribution and crystallization quality of the CVD layer under different growth conditions were compared, and the growth process of the high-quality single crystal diamond was optimized.

2. Experimental details

Single crystal diamonds were grown using a 2.45 GHz, 5 kW microwave plasma CVD reactor. The growth temperature was measured with an infrared radiation thermometer (SCIT-1M2 Infrared thermometer). The seed substrate was (001) oriented 4.0 mm × 4.0 mm × ~ 1.0 mm high pressure, high temperature (HPHT) type Ib synthetic single crystal diamond. The substrate was cleaned with acetone in an ultrasonic bath and put into the reactor with the substrate holder. The reactor system was pumped for 1.5 h to reach a base pressure of ~ 10^{-4} Pa. High-purity hydrogen (6N) and methane (6N) gases were used as the process gas. Then, the seed substrate was etched in the plasma for 30 min under H_2 flows of 300 sccm and flows of 6 sccm for O_2. The size relationship between the seed substrate and the square holes of the shielding ring were optimized. The input microwave power during the growth was 2.6–2.9 kW. The pressure of the reactor was 25–27 kPa, and the gas flow rate was 300 sccm for H_2, 5% of the H_2 flow for CH_4. The grown sample was laser cut to separate the CVD layer from the seed substrate. The CVD layer was then polished, and the surface roughness of the CVD layer after polishing was about 5 nm.

The surface morphology of the grown diamond was characterized using a Keyence VHX-6000 3D Digital Microscope. Birefringence photographs of the CVD layers were measured with an Olympus BX51 microscope. The crystalline quality was characterized by the diamond (400) rocking curve of the Philips X′Pert MRD Diffractometer high resolution via X-ray diffraction using a monochromized Cu-Kα_1 X-ray source with a Ge (220) four-crystal monochromator.

An X-ray white topography test was carried out on the HPHT type Ib seed substrate and the grown CVD layer, respectively. The main parameters of the test were as follows: the distance from the sample to the film was 5.5 cm; the film was produced by FUJI KOGYO, and the film model was FUJI-IX50; the storage ring operating parameters were 2.5 GeV and 250 mA; and the

distance of the sample from the light source was about 42 meters.

3. Results and discussion

3.1 The growth of the single crystal diamond

Fig. 1 shows a schematic diagram of the molybdenum holder. The seed substrate is placed on the seed substrate holder. The edge effect of the microwave electric field on the seed substrate is reduced by the shielding effect of the shielding ring, which improves the local controllability of single crystal diamond synthesis. The seed substrate must be a suitable thermal environment that supports a uniform single crystal synthesis process. The size of the shielding ring is important, and its dimensions control the local synthesis. An inappropriate space relationship between the square hole of the shielding ring and the seed substrate is not conducive to obtaining a single crystal diamond with a smooth surface.

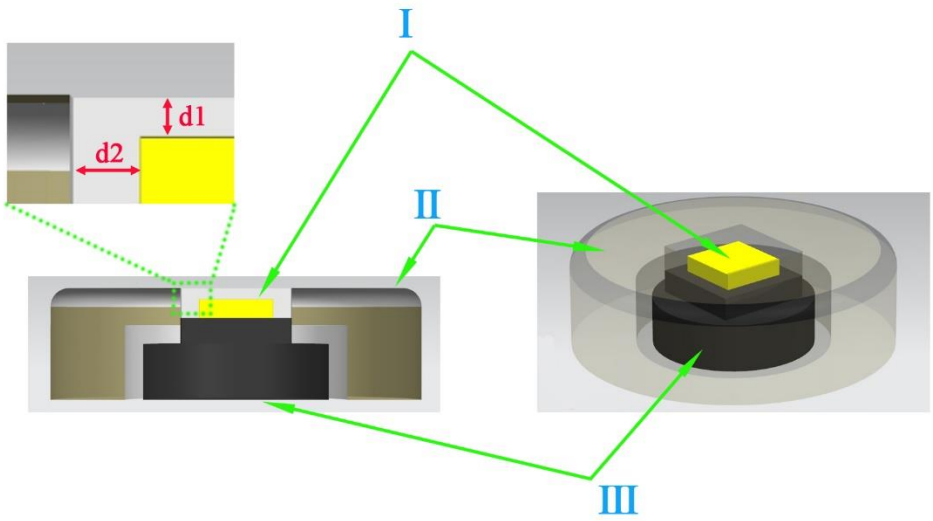

Fig. 1. Molybdenum holder diagram for growth of seeded substrate. I Seed substrate, II Shield ring, III Seed substrate holder. The upper left corner of the picture is a magnified view of the corresponding relationship of the size between the seed substrate and the square hole of the shielding ring. d1 is the distance between the surface of the seed substrate and the top surface of the shielding ring. d2 is the distance between the side surface of the seed substrate and the inner wall of the square hole of the shielding ring.

The seed substrates were grown with different sizes of shielded ring holes. Based on the surface morphology of the as-grown samples, the optimized size relationship between the seed substrate and the square hole of the shielding ring was obtained. The dimensions represented by d1 and d2 are shown in Fig. 1. The surface morphologies of the samples grown at different d1/d2 values are shown in Fig. 2. When d1/d2 is equal to 0.7, the surface quality of the as-grown sample is better. As shown in Fig. 2 (d), the sample was grown for 50 h and obtained a thickness of ~ 1 mm, and the growth surface of the sample was smooth and flat with little or no polycrystalline edge. As shown in Fig. 2 (a)–(c), when the value of d1/d2 is small, either the edge of the sample is covered with polycrystalline diamond and the surface appears poly-crystallization or the growth surface is not flat, with a growth morphology from the edge to the center, which reduces the surface areas of the samples. Fig. 2 (e) shows that when the d1/d2 value is large, although there is

no polycrystalline diamond on the edge of the sample, the growth morphology is two-dimensional extended growth, which is not conducive to the growth of high-quality single crystal diamonds. Fig. 3 (a), (b), and (c) are magnified views of the surface of the samples in Fig. 2 (a), (d), and (e), respectively. When d1/d2 is equal to 0.7, a uniform step-flow growth morphology appears on the sample surface, as shown in Fig. 3 (b).

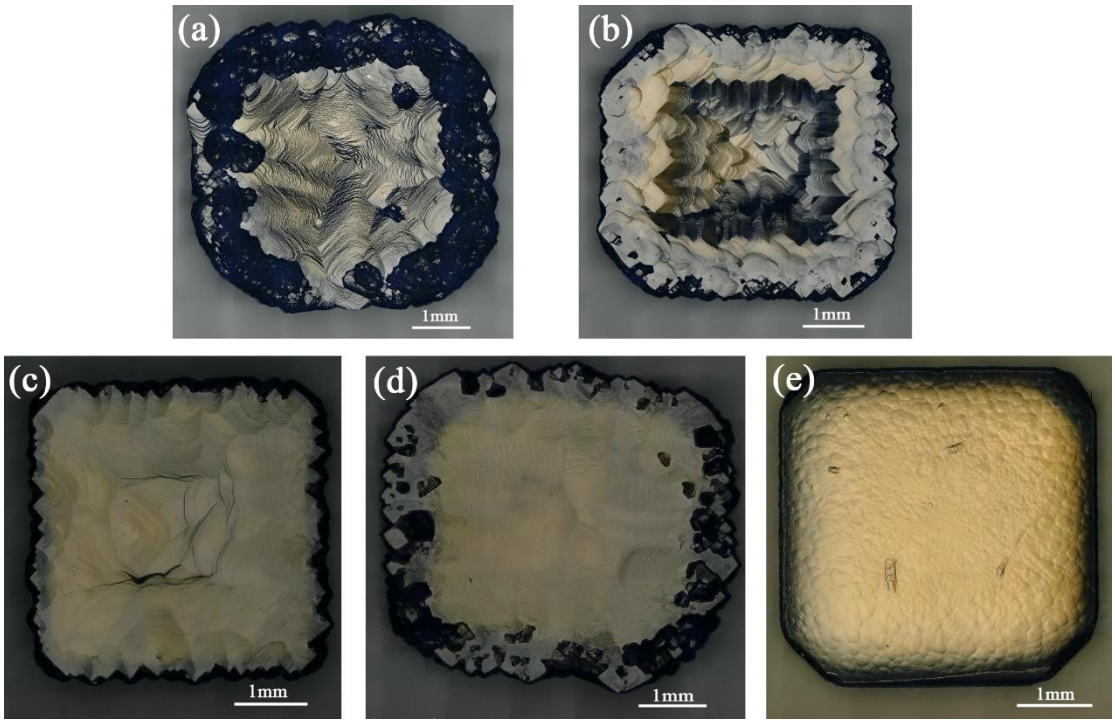

Fig. 2. The growth morphology of the samples at different d1/d2 values. (a) d1/d2=0.1; (b) d1/d2=0.3; (c) d1/d2=0.5; (d) d1/d2=0.7; (e) d1/d2=0.9.

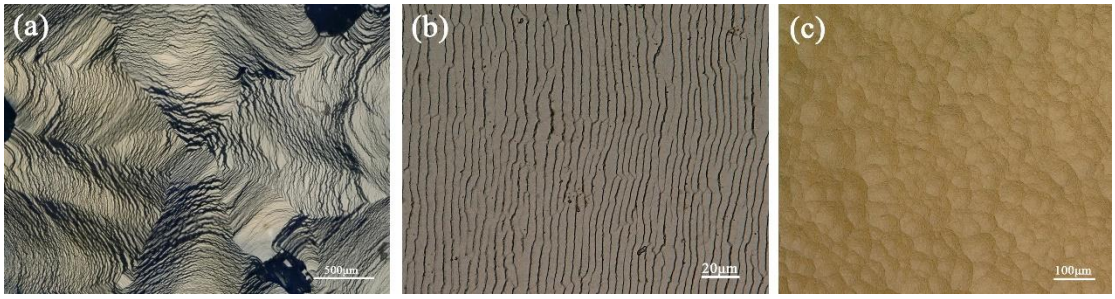

Fig. 3. (a), (b), and (c) are magnified views of the surface of the samples in Fig. 2 (a), (d), and (e), respectively. (a) The morphology of the growth from the edge to the center. (b) The growth morphology of uniform step flow. (c) The growth morphology of two-dimensional extended growth.

While the single crystal CVD layer was grown on the substrate surface, a polycrystalline diamond was also generated at the edge of the substrate to form a polycrystalline edge. In addition, the thickness of both the CVD layer and the polycrystalline edge increased, while the growth surface of the single crystal diamond exhibited a center-to-edge morphology. At the same time, the polycrystalline edge of the sample grew outward horizontally, and the surface area did not decrease. Fig. 4 (a) shows the surface morphology of sample 1 after 50 h of growth, and the growth thickness of the sample is 1 mm. As the growth proceeds, the thicker polycrystalline layer

grows on the surface of the shield ring and connects to the edge of the sample. At this point, the surface of the sample is almost flush with the polycrystalline layer grown on the shield ring. The thickness of the CVD layer continues to increase as the growth progresses, and the surface of the sample extends deeper into the plasma. The sample has exceeded the polycrystalline film, and the edge effect of the sample is more obvious, which results in a change in the uniformity of the surface temperature of the sample. Moreover, the thickness of the polycrystalline edge begins to be greater than the thickness of the single crystal surface. When the polycrystalline edge of the substrate extends deep into the plasma, the state of the boundary layer between the substrate and the plasma changes [23]. This changes the growth conditions, which in turn aggravates the inhomogeneity of the surface temperature of the sample. That is, when the surface of the diamond exhibits an edge-to-center morphology, the surface becomes uneven. Fig. 4 (b) shows the surface morphology of sample 2 after 69 h of growth, and the thickness of the sample is 1.4 mm. As shown in Fig. 4 (c) and (d), the difference in height between the center and the edge of sample 2 is 112 μm, and the surface area is 17% less than the original surface area of the seed substrate.

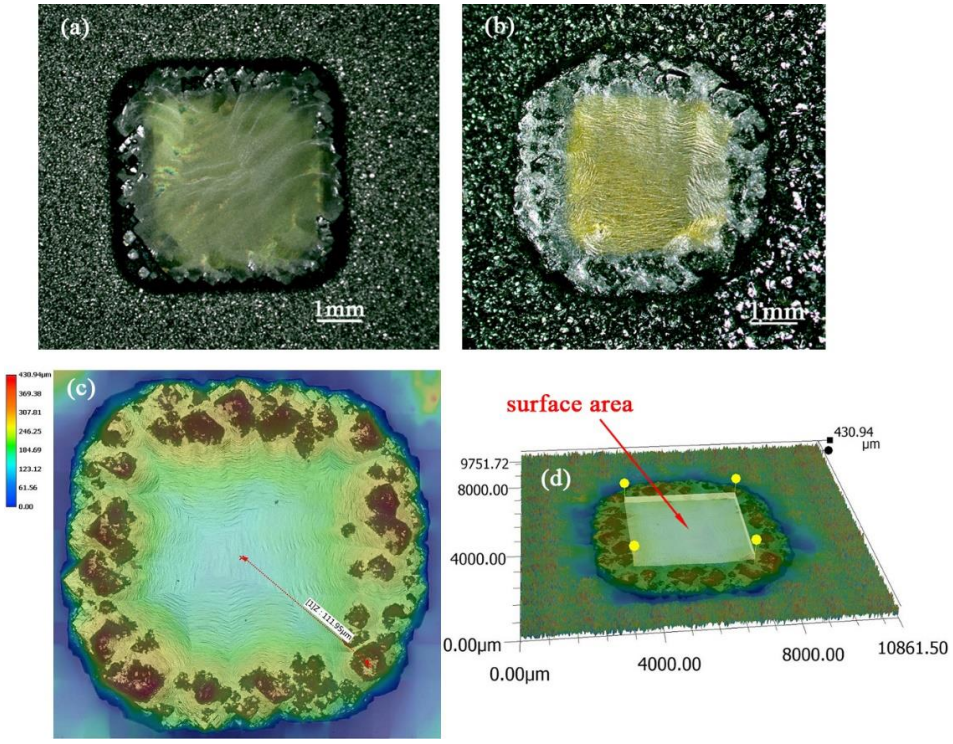

Fig. 4. Morphology change of the growth surface of the single crystal diamond. (a) After the growth of sample 1 for 50 h, the thickness increased by 1 mm, and the surface of the sample was flush with the polycrystalline film. (b) After the growth of sample 2 for 69 h, the thickness increased by 1.4 mm, and the surface of the sample exceeded the polycrystalline film. The polycrystalline edge is higher than the center of the sample surface, showing an edge-to-center growth morphology. (c) The difference in height between the center and the edge of sample 2 is 112 μm. (d) The surface area with no polycrystalline edge of sample 2, which is 17% less than the original surface area of the seed substrate.

3.2 Quality analysis of the CVD layers

Single crystal diamonds grown by CVD often exhibit strain-induced birefringence arising from bundles of dislocation [27,28]. CVD layer 1 and CVD layer 2 grown from sample 1 and

sample 2 were polished to the same thickness. Both CVD layers exhibit high-order anomalous birefringence under crossed polarizers, as shown in Fig. 5. The full width at half maximum (FWHM) of rocking curves for CVD layer 1 and CVD layer 2 are 0.013° and 0.032°, respectively, as shown in Fig. 6. The dislocation densities calculated according to formula [29] are 8.3×10^6 cm^{-2} and 5.3×10^7 cm^{-2}, respectively. It is found that the dislocation density is higher as the higher-order anomalous birefringence becomes more obvious. This shows that the higher-order anomalous birefringence of the samples has a corresponding relationship with the dislocation density. The higher the dislocation density of the sample, the greater the stress and strain, and the higher-order anomalous birefringence of the sample is more pronounced (appeared red, green, yellow, etc.). The strain field of a bundle of dislocations can be found using isotropic elasticity theory. The intensity of birefringence $I=E^2\sin^2(2\varphi)\sin^2(\delta/2)$, where φ is angle between a principal axis of strain and a polarizer and δ is the phase difference between the two polarized components of the light ray at the exit of the diamond [30]. The phase difference $\delta=2\pi\ (n_1 - n_2)\ t/\lambda$, where n_1 and n_2 are the refractive indices of the diamond along the principal directions of strain, t is the optical thickness of the CVD layer which is 0.8 mm, and λ is the wavelength of mercury lamp which is 550 nm. The refractive indices are related to the strain through the strain-optic coefficient p_{ij}, and $n_1 - n_2 = -n^3\ (p_{11} - p_{12})\ (\epsilon'_{11} - \epsilon'_{12})/2$, where $p_{11} - p_{12}$ is equal to -0.3 [27,31], and ϵ'_{ii} are the principal values of the strain tensor and n is the refractive index of the diamond, so δ is related to the shear strain $(\epsilon'_{11} - \epsilon'_{12})/2$. Therefore, the strain field is proportional to δ that gives the different shear strain field in the different regions of the CVD layer [27].

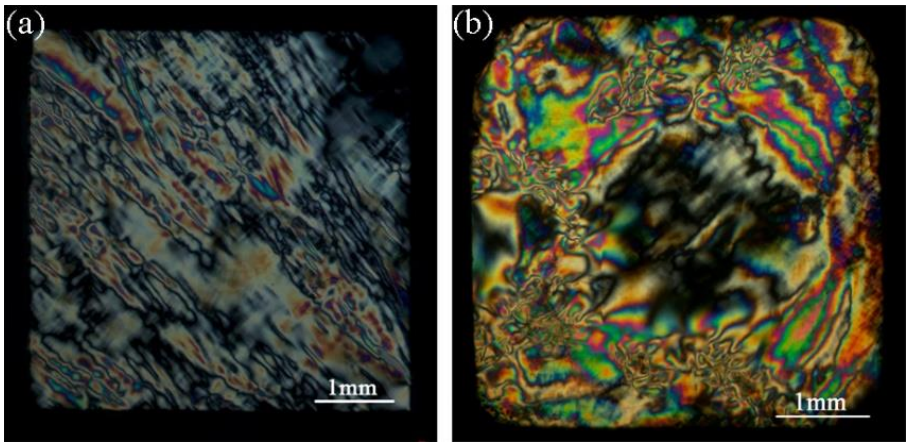

Fig. 5. Birefringence photographs of CVD layers with the same thickness obtained after grinding and polishing. (a) Birefringence photograph of CVD layer 1 of sample 1. (b) Birefringence photograph of CVD layer 2 of sample 2.

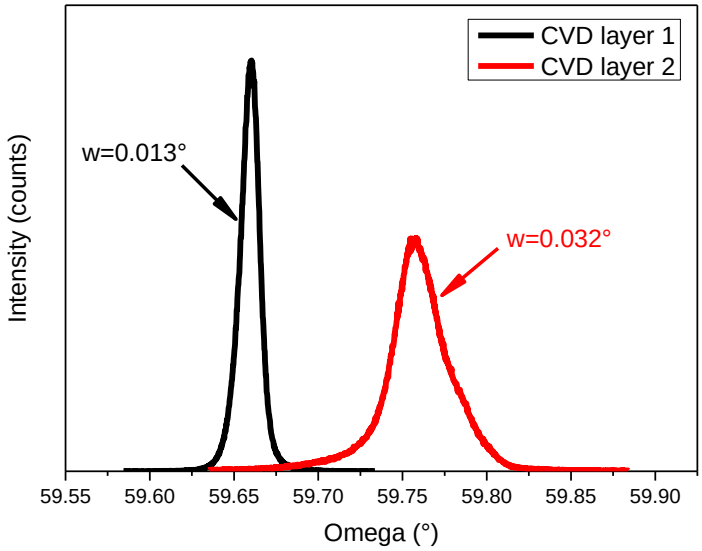

Fig. 6. The rocking curves of CVD layer 1 and CVD layer 2, respectively, grown on sample 1 and sample 2, and the FWHM is 0.013° and 0.032°, respectively.

The birefringence photograph in Fig. 5 (b) shows that the stress in the middle region of the CVD layer 2 is lower than the stress around it. This phenomenon is related to the growth of sample 2. X-ray white topography is a method used to examine the microstructure defects of crystal material, and it is widely used in the study of the integrity of crystal material [32-34]. Fig. 7 (a) shows an X-ray white morphology image of HPHT type Ib seed substrate, showing the defects of the seed substrate and their distribution. And these defects have been marked, I dislocations, for single crystal diamonds, the dislocations are more easily distributed in the (111) growth sector, II growth sector boundaries, III stacking faults, IV strain field of inclusion. Most of these defects are distributed outside the (100) growth sector, that is, the edge of the seed substrate. Fig. 7 (b) shows the surface morphology of sample 2, as observed from the side. The surface morphology is similar to an inverted pyramid pit, and the surface is grown in step flow. The schematic diagram of a cross-section of sample 2 along the growth direction is shown in Fig. 7 (c), and the direction of dislocation propagation in the CVD layer has changed. When the epitaxial CVD layer grows out of polycrystalline diamond on the shielding ring, the thickness of the polycrystalline edge of the sample becomes greater than the thickness of its surface. The surface becomes uneven and shows an edge-to-center growth morphology. The dislocations in the CVD layer above the yellow dashed line begin to bend and converge to the central area, as shown in Fig. 7 (c).

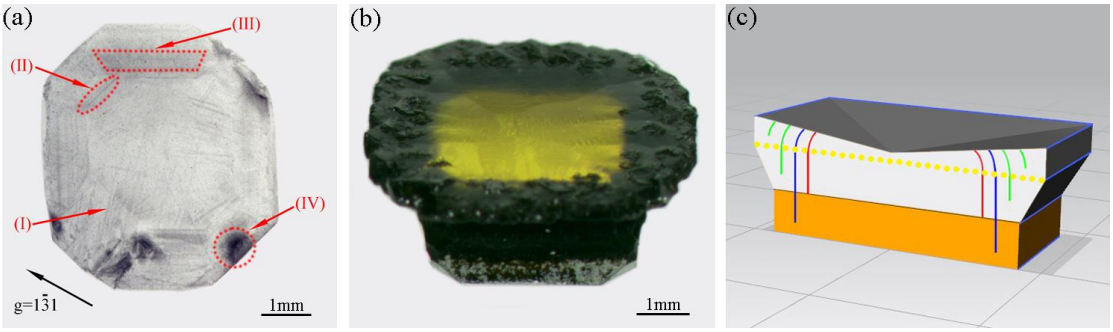

Fig. 7. (a) X-ray white topography image of the seed substrate. The defects in the seed substrate have been marked, I dislocations, II growth sector boundaries, III stacking faults, IV strain field of inclusion. (b) The surface morphology of sample 2, as observed from the side. The surface morphology is similar to an inverted pyramid pit, and the surface is grown in step flow. (c) A schematic diagram of the propagation of dislocation in the epitaxial CVD layer of sample 2. Blue lines represent dislocations originating in the seed substrate, while red lines represent dislocations originating from the substrate surface. Green lines represent dislocations generated during the growth of the CVD layer. When the edge of the sample is higher than the center, the dislocations in the CVD layer above the yellow dashed line gather toward the center.

Fig. 8 shows X-ray white topography images of CVD layer 2. The area of the blue dashed line is the central area of CVD layer 2, and its dislocation density is lower than that of the edge, so a low stress zone is formed in the central area, as shown in Fig. 8 (a). In Fig. 8 (b), the green dashed line indicates the direction of propagation of the dislocations in CVD layer 2, and the dislocation lines have been bent and gathered to the central area.

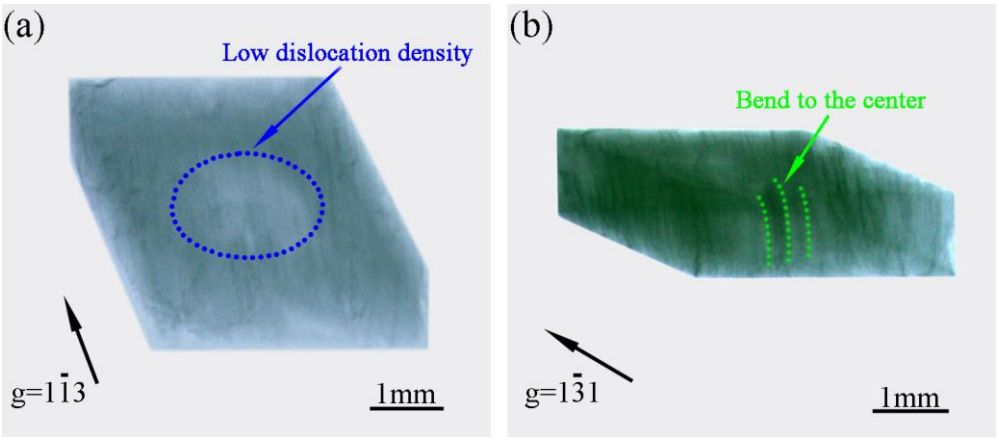

Fig. 8. X-ray white topography images of CVD layer 2. (a) The blue dashed area is the central area of CVD layer 2, with a relatively low dislocation density. (b) The green dashed line indicates the direction of propagation of the dislocations in CVD layer 2. The dislocation lines have been bent and gathered to the central area.

In order to further analyze the crystal quality of CVD layer 2, the Rocking curve mapping test was conducted. Fig. 9 shows the Phi–Omega mapping of CVD layer 2; the inset shows the Psi–Omega mapping for the corresponding plot. The scan steps were ω = 0.0004°, Phi = 10°, Psi = 0.03°, and the Omega scan range is 58.05°–59.94°. It can be seen from the inset of Fig. 9 that the Psi–Omega mapping of CVD layer 2 is not perfectly symmetrical, and the highest intensity is biased to the left, which indicates that the surface orientation of CVD layer 2 is not exactly the same, and there is a small angle deviation. High dislocation density leads to a mosaic structure and orientation deviation [35].

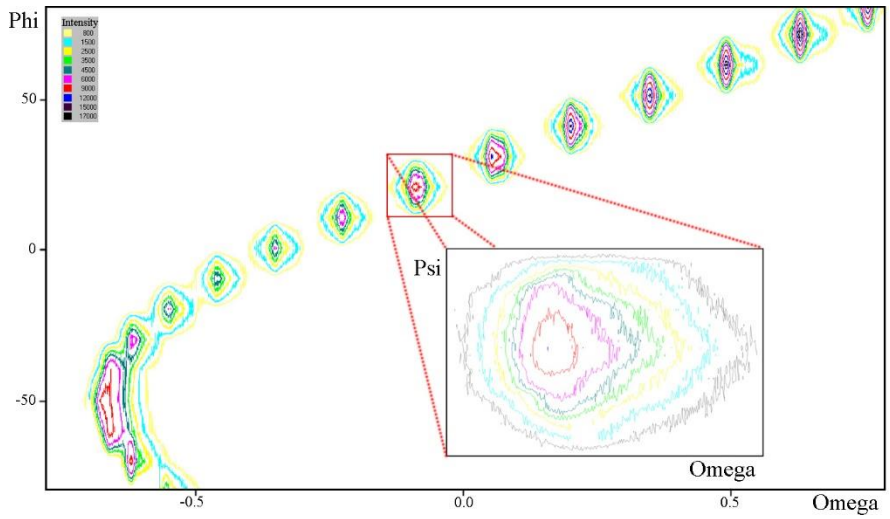

Fig. 9. Phi–Omega mapping of CVD layer 2; the inset shows the Psi–Omega mapping for the corresponding plot.

4. Conclusion

The seed substrate is placed in a molybdenum holder with a shield ring. The state of the boundary layer between the seed substrate and the plasma is changed by optimizing the size relationship between the seed substrate and the square hole of the shielding ring. Hence, the surface and edge of the seed substrate are in a relatively uniform heat environment, inhibiting the formation of a polycrystalline diamond on the surface of the seed substrate. At the same time, the growth surface becomes smooth and flat. This may not result in the growth of a high-quality single crystal diamond but also greatly increase the growth thickness. After 50 h of growth, the thickness of the sample increases by 1 mm, and the surface exhibits uniform step flow growth morphology. After 69 h of growth, the thickness of the sample increases by 1.4 mm, but the surface shows an edge-to-center morphology. The difference in height of the center and edge of the sample reaches 112 μm, and the surface area decreases by 17% compared with the original seed.

The CVD layers grown at different times were polished to the same thickness. Due to high dislocation density, the internal stress and strain are larger, and high-order anomalous birefringence appears in both CVD layers. Dislocations of the CVD layer grown from the edge to the center are bent, and the dislocations converge toward the central area. A small low-stress zone is formed in the central region. The high dislocation density causes a small angular deviation in the lattice orientation of the CVD layer, which forms a mosaic structure.

Acknowledgments

The authors wish to thank the staff members of 4W1A beamline of Beijing Synchrotron Radiation Facility for corresponding experiments and discussion. This work was supported by the National Key Research and Development Program of China (No. 2016YFE0133200) and European Union's Horizon 2020 Research and Innovation Staff Exchange (RISE) Scheme (No. 734578). The authors are very grateful for their financial support.

References

[1] A. Tallaire, J. Achard, F. Silva, O. Brinza, A. Gicquel, Growth of large size diamond single crystals by plasma assisted chemical vapour deposition: Recent achievements and remaining challenges, C. R. Physique 14 (2-3) (2013) 169-184.
[2] M. Schreck, J. Asmussen, S. Shikata, J. C. Arnault, N. Fujimori, Large-area high-quality single crystal diamond, Mrs Bulletin 39 (6) (2014) 504-510.
[3] S. Shikata, Single crystal diamond wafers for high power electronics, Diam. Relat. Mater. 65 (2016) 168-175.
[4] H. Umezawa, Y. Kato, S. I. Shikata, 1 Ω on-resistance diamond vertical-Schottky barrier diode operated at 250 °C, Appl. Phys. Express, 6 (1) (2012) 011302.
[5] S. Terentyev, M. Polikarpov, I. Snigireva, M. Di Michiel, S. Zholudev, V. Yunkin, A. Snigirev, Linear parabolic single-crystal diamond refractive lenses for synchrotron X-ray sources, J. Synchrotron Rad. 24 (1) (2017) 103-109.
[6] R. P. Mildren, A. Sabella, O. Kitzler, D. J. Spence, A. M. McKay, Diamond Raman laser design and performance, Optical Engineering of Diamond, 2013 239-276.
[7] I. Zamboni, Ž. Pastuović, M. Jakšić, Radiation hardness of single crystal CVD diamond detector tested with MeV energy ions, Diam. Relat. Mater. 31 (2013) 65-71.
[8] T. Kononenko, V. Ralchenko, A. Bolshakov, V. Konov, P. Allegrini, M. Pacilli, E. Spiriti, All-carbon detector with buried graphite pillars in CVD diamond, Appl. Phys. A 114 (2) (2014) 297-300.
[9] G. Balasubramanian, I. Y. Chan, R. Kolesov, M. Al-Hmoud, J. Tisler, C. Shin, T. Hanke, Nanoscale imaging magnetometry with diamond spins under ambient conditions, Nature 455 (7213) (2008) 648-651.
[10] F. Dolde, I. Jakobi, B. Naydenov, N. Zhao, S. Pezzagna, C. Trautmann, J. Wrachtrup, Room-temperature entanglement between single defect spins in diamond, Nature Physics 9 (3) (2013) 139-143.
[11] L. Childress, R. Hanson, Diamond NV centers for quantum computing and quantum networks, MRS bulletin 38 (2) (2013) 134-138.
[12] S. Stoupin, Novel diamond X-ray crystal optics for synchrotrons and X-ray free-electron lasers, Diam. Relat. Mater. 49 (2014) 39-47.
[13] M. Polikarpov, I. Snigireva, J. Morse, V. Yunkin, S. Kuznetsov, A. Snigirev, Large-acceptance diamond planar refractive lenses manufactured by laser cutting, J. Synchrotron Rad. 22 (1) (2015) 23-28.
[14] E. V. Bushuev, V. Y. Yurov, A. P. Bolshakov, V. G. Ralchenko, A. A. Khomich, I. A. Antonova, V. I. Konov, Express in situ measurement of epitaxial CVD diamond film growth kinetics, Diam. Relat. Mater. 72 (2017) 61-70.
[15] A. M. Zaitsev, W. Wang, K. S. Moe, P. Johnson, Spectroscopic studies of yellow nitrogen-doped CVD diamonds, Diam. Relat. Mater. 68 (2016) 51-61.
[16] J. Achard, F. Silva, O. Brinza, A. Tallaire, A. Gicquel, Coupled effect of nitrogen addition and surface temperature on the morphology and the kinetics of thick CVD diamond single crystals, Diam. Relat. Mater. 16 (2007) 685-689.
[17] M. A. Lobaev, A. M. Gorbachev, S. A. Bogdanov, A. L. Vikharev, D. B. Radishev, V. A. Isaev, M. N. Drozdov, Influence of CVD diamond growth conditions on nitrogen incorporation, Diam. Relat. Mater. 72 (2017) 1-6.
[18] A. Tallaire, J. Achard, O. Brinza, V. Mille, M. Naamoun, F. Silva, A. Gicquel, Growth

strategy for controlling dislocation densities and crystal morphologies of single crystal diamond by using pyramidal-shape substrates, Diam. Relat. Mater. 33 (2013) 71-77.
[19] M. Naamoun, A. Tallaire, P. Doppelt, A. Gicquel, M. Legros, J. Barjon, J. Achard, Reduction of dislocation densities in single crystal CVD diamond by using self-assembled metallic masks, Diam. Relat. Mater. 58 (2015) 62-68.
[20] A. Tallaire, V. Mille, O. Brinza, T. N. T. Thi, J. M. Brom, Y. Loguinov, J. Achard, Thick CVD diamond films grown on high-quality type IIa HPHT diamond substrates from New Diamond Technology, Diam. Relat. Mater. 77 (2017) 146-152.
[21] B. Willems, A. Tallaire, J. Achard, Optical study of defects in thick undoped CVD synthetic diamond layers, Diam. Relat. Mater. 41 (2014) 25-33.
[22] H. Yamada, A. Chayahara, Y. Mokuno, Y. Horino, S. Shikata, Simulation of microwave plasmas concentrated on the top surface of a diamond substrate with finite thickness, Diam. Relat. Mater. 15 (9) (2006) 1383-1388.
[23] S. Nad, Y. Gu, J. Asmussen, Growth strategies for large and high quality single crystal diamond substrates, Diam. Relat. Mater. 60 (2015) 26-34.
[24] G. Wu, M. H. Chen, J. Liao, The influence of recess depth and crystallographic orientation of seed sides on homoepitaxial growth of CVD single crystal diamonds, Diam. Relat. Mater. 65 (2016) 144-151.
[25] A. Charris, S. Nad, J. Asmussen, Exploring constant substrate temperature and constant high pressure SCD growth using variable pocket holder depths, Diam. Relat. Mater. 76 (2017) 58-67.
[26] H. Yamada, A. Chayahara, Y. Mokuno, Y. Horino, S. Shikata, Simulation of temperature and gas flow distributions in region close to a diamond substrate with finite thickness, Diam. Relat. Mater. 15 (10) (2006) 1738-1742.
[27] H. Pinto, R. Jones, Theory of the birefringence due to dislocations in single crystal CVD diamond, J. Phys.: Condens. Matter 21 (36) (2009) 364220.
[28] A. Crisci, F. Baillet, M. Mermoux, G. Bogdan, M. Nesládek, K. Haenen, Residual strain around grown ‐ in defects in CVD diamond single crystals: A 2D and 3D Raman imaging study, Phys. status solidi A 208 (9) (2011) 2038-2044.
[29] A. D. Kurtz, S. A. Kulin, B. L. Averbach, Effect of dislocations on the minority carrier lifetime in semiconductors, Phys. Rev. 101 (4) (1956) 1285.
[30] M. Born, E. Wolf, Principles of optics: electromagnetic theory of propagation, interference and diffraction of light, Elsevier, 2013.
[31] L. S. Hounsome, R. Jones, M. J. Shaw, P. R. Briddon, Photoelastic constants in diamond and silicon, physica status solidi (a), 203 (2006) 3088.
[32] A. R. Lang, Space-filling by branching columnar single-crystal growth: An example from crystallisation of diamond, J. Cryst. Growth 23 (2) (1974) 151-153.
[33] A. R. Lang, Topographic methods for studying defects in diamonds, Diam. Relat. Mater. 2 (2-4) (1993) 106-114.
[34] T. N. Tran Thi, J. Morse, D. Caliste, B. Fernandez, D. Eon, J. Härtwig, T. A. Lafford, Synchrotron Bragg diffraction imaging characterization of synthetic diamond crystals for optical and electronic power device applications, J. Appl. Cryst. 50 (2) (2017) 561-569.
[35] A. F. Khokhryakov, D. V. Nechaev, Y. N. Palyanov, K. E. Kuper, The dislocation structure of diamond crystals grown on seeds in the Mg-C system, Diam. Relat. Mater. 70 (2016) 1-6.